Front. Earth Sci. 2023, 17(1): 45−57
https://doi.org/10.1007/s11707-022-1012-3

RESEARCH ARTICLE

Experimental and numerical study of coal mechanical properties during coalification jumps

Qiang HUANG[1], Xuehai FU[1], Jian SHEN (✉)[1], Qiangling YAO[2], Ming CHENG[1]

1 Key Laboratory of Coalbed Methane Resources & Reservoir Formation Process (Ministry of Education), China University of Mining and Technology, Xuzhou 221116, China
2 School of Mines, Key Laboratory of Deep Coal Resource Mining, Ministry of Education, China University of Mining & Technology, Xuzhou 221116, China

Abstract The mechanical characteristics of coal reservoirs are important parameters in the hydraulic fracturing of coal. In this study, coal samples of different ranks were collected from 12 coal mines located in Xinjiang and Shanxi, China. The coal ranks were identified with by the increased Maximum vitrine reflectance ($R_{o,max}$) value. The triaxial compression experiments were performed to determine the confining pressure effect on the mechanical properties of coal samples of different ranks. The numerical approaches, including the power function, arctangent, and exponential function models, were used to find the correlation between coal elastic modulus and the confining pressure. The fitting equations of compressive strength and elastic modulus of coal ranks were constructed under different confining pressures. The results showed that the coal compressive strength of different ranks has a positive linear correlation with the confining pressure. The coal elastic modulus and confining pressure showed an exponential function. Poisson's ratio of coal and confining pressure show negative logarithmic function. The stress sensitivity of the coal elastic modulus decreases with the increase of confining pressure. The coalification jump identifies that the compressive strength, elastic modulus, and stress sensitivity coefficient of coal have a polynomial relationship with the increase of coal ranks. The inflection points in coalification at $R_{o,max}$ = 0.70%, 1.30%, and 2.40%, are the first, second, and third coalification jumps. These findings provide significant support to coal fracturing during CBM production.

Keywords compressive strength, elastic modulus, confining pressure, Poisson's ratio, coalification jump

Received March 3, 2022; accepted May 19, 2022

E-mail: jianshen@cumt.edu.cn

1 Introduction

Coal reservoirs in China generally have characteristics of low porosity and low permeability, and a fracture network is usually developed in coal seams through hydraulic fracturing for the Coalbed Methane (CBM) recovery (Su et al., 2004; Liu et al., 2018; Li et al., 2021). The elastic modulus, Poisson's ratio, and compressive strength are important mechanical parameters to measure the deformation and failure characteristics of coal reservoirs during the fracturing process. The elastic modulus measures the rigidity or stiffness of the coal under a given strain. The Poisson's ratio is dimensionless and measures the deformation of coal under applied stress. The compressive strength measures the ability of the coal under the maximum applied strain that coal can sustain without fracture (Peng et al., 2009; Xiong et al., 2014; Perera et al., 2016; Meszaros et al., 2017). The deeply buried seams and evolution of coal significantly affect the mechanical properties of the coal (Pan et al., 2013; Jiang et al., 2016; Zhang et al., 2019a). The mechanical parameters are also influenced by the physical and chemical properties of the coal under the confining pressure during the coalification jump process and provide theoretical guidance for the formulation of fracturing schemes for reservoirs of different coal ranks.

Triaxial mechanics experiment is a standard method to analyze the mechanical properties of coal and rock in the laboratory. Scholars have conducted many experimental studies (Masoudian et al., 2014; Yao et al., 2015; Hobbs, 1960). Previously reported studies showed a positive linear correlation between the compressive strength of the coal and the confining pressure, whereas the elastic modulus has a nonlinear relationship with the confining pressure (Gentzis et al., 2007; Hobbs, 1960; Zhang et al., 2020a). Hobbs (2009) conducts triaxial compression experiments on coals of different ranks and found that the

elastic modulus tends to be stable when the confining pressure exceeds 7 MPa. On the other hand, Masoudian et al. (2014) believes that the confining pressure closes the fractures in the coal and alters coal compression process; as a result, the elastic modulus of the coal sample shows different trends with the confining pressure. Gentzis et al. (2007) found that the slopes of the elastic modulus-confining pressure curves of six bituminous coal samples decreased, and the elastic modulus of the coal changes in stages with the increase in confining pressure. According to Yu et al. (1993), coal elastic modulus has a nonlinear relationship with the confining pressure, and elastic modulus tends to be stable with the confining pressure. According to You (2003), coal structure is elastic and has weak planes. The elastic modulus increases with the confining pressure, and weak planes in the coal become closed. The coal becomes completely elastic with the further increase in the confining pressure, and the elastic modulus does not change anymore.

Pan et al. (2013) and Zhang et al. (2020a) reported that compressive strength and elastic modulus vary significantly with the different coal ranks. The moisture content changes the mechanical characteristics of different coal ranks significantly, as reported by Yao et al. (2015) and Yang et al. (2020). According to Ranathunga et al. (2016), the fissure density also significantly changes the mechanical strength of coal samples with different ranks.

Lin et al. (2022) and Zhang et al. (2020a) reported that the water content, fissure density, porosity, and matrix compressibility of coal are all influenced by the coalification transition, which significantly affects the mechanical properties of coal (Zhou et al., 2018). Specifically, before the first coalification jump, the water content dropped sharply, and the coal porosity gradually decreased due to the compaction of the overlying rock (Zhou et al., 2017; Lin et al., 2022). Between the first and second transition points, the density of the internal fractures of the coal gradually increases, and the porosity decreases continuously due to the influence of the high pressure during the asphaltization, aromatization, and coalification processes (Wang et al., 2019; Xin et al., 2019; Hou et al., 2020). After the third transition point, the methyl groups and hydroxyl groups on the coal chemical skeleton decrease significantly due to thermal crack, and the coal seam water content further increases (Zhang et al., 2019a; Yan et al., 2021).

In the past, predecessors have carried out many studies on the relationship between elastic modulus and confining pressure, but the study mostly uses the coal samples of the same rank coals and pays less attention to the differences of different rank coals (Hobbs, 1960; Gentzis et al., 2007; Liu et al., 2018; Zhang et al., 2019a), and the effect of the physical properties of coal on mechanical parameters in the process of coalification jump is still unclear. In this study, we have performed triaxial compression experiments and measured the correlation between elastic modulus and the confining pressure to predict the impact on mechanical properties of coal by adopting different numerical approaches, such as power function, arctangent function, and exponential function model. The fitting equations of elastic modulus with confining pressure and strength criteria of different rank coals have been constructed to study their mechanical impact on coalification. Furthermore, the elastic modulus stress sensitivity coefficient and strength coefficient describe the deformation and failure characteristics of coals of different ranks to understand the coal fracturing for CBM production.

2 Samples and methods

2.1 Samples

The samples were collected from different coal mines in Xinjiang and Shanxi, China. The samples were abbreviated based on the name of their respective coal mines. The Tongtai Coal Mine (TT) lignite in Keer alkali mining district, Tuha Basin, and gas coal of Xiaogangou Coal Mine (XGG) in the Fukang mining area, Zhunnan coalfield, are located in Xinjiang. The long flame coal was collected from Shaping coal mine (SP) in the Hedong coalfield, fat coal was taken from Liyazhuang coal mine (LYZ) in the Huoxi coalfield, and coal was sampled from Huaian (HA), Xinzhuang (XZ), Shibangou (SBG), Yeucheng (YC), Yangquan (YQWK) coal mines in Qinshui coalfield of Shanxi, China. The collected coal samples were quickly wrapped in plastic. A 50 mm × 100 mm sized cylindrical sub-sample was drilled along the bedding direction of each coal sample. The processing accuracy of the coal samples was done according to the International Society of Rock Mechanics (ISRM) standards (Fig. 1). All the experiments were performed on the adjacent uniform columns derived from the cylindrical samples of each coal mine. The surface of the column was intact to reduce the influence of coal heterogeneity and the interference of external factors.

The proximate and ultimate analyses of coal samples are given in Table 1. The maximum reflectance of vitrinite ($R_{o,max}$) of coal samples under oil immersion conditions is between 0.34%–3.04% indicating coal ranks

Fig. 1 Coal samples for triaxial mechanics.

Table 1 The coal petrology and proximate analysis

Samples	Location	Coalfield	Macrolithotype	$R_{o,max}$/%	Maceral			Industrial analysis		
					V/%	I/%	L/%	M_{ad}/%	A_{ad}/%	V_{daf}/%
TT	Tongtai	Keer alkali	Bleak coal	0.34	18.58	79.78	1.64	3.12	4.95	65.18
SP	Shaping	Hedong	Semidull coal	0.59	55.44	42.13	2.43	4.18	24.07	50.51
XGG	Xiaogangou	Fukang	Semidull coal	0.67	35.22	63.53	1.25	0.80	10.89	58.54
LYZ	Liyazhuang	Huoxi	Semidull coal	0.97	42.07	53.66	4.27	0.66	4.01	69.78
HA	Huaian	Qinshui	Semidull coal	1.54	50.84	47.36	1.80	0.98	12.65	67.32
SYFD	Sanyuanfuda	Qinshui	Bright coal	1.59	86.59	13.41	0.00	1.01	3.82	80.72
DZ	Dongzhuang	Qinshui	Semibright coal	1.63	68.88	31.12	0.00	0.66	19.45	57.76
WZ	Wenzhuang	Qinshui	Semibright coal	1.73	68.31	31.69	0.00	1.12	5.24	79.60
XZ	Xinzhuang	Qinshui	Semibright coal	1.88	82.30	17.40	0.30	0.82	24.20	53.22
SBG	Shibangou	Qinshui	Bright coal	1.97	87.75	11.15	1.10	1.51	15.23	70.27
YC	Yuecheng	Qinshui	Semibright coal	2.80	70.56	29.31	0.13	1.50	15.61	78.11
YQWK	Yangquan	Qinshui	Semibright coal	3.04	65.77	34.23	0.00	2.73	6.37	85.24

Notes: $R_{o,max}$, Maximum vitrinite reflectance, %; V, Vitrinite, %; I, inertinite, %; L, Liptinite, %; M_{ad}, moisture content of air-drying basis, %; A_{ad}, ash yields of air-drying basis, %; V_{daf}, dry-ash-free volatile component, %; The data of samples SYFD, DZ, WZ is cited from Zhang et al. (2020c).

from lignite to anthracite, the moisture content of air-drying basis (M_{ad}) is between 0.66%–4.18%, ash yields (A_{ad}) is 4.01%–20.20%, and the dry-ash-free volatile component (V_{daf}) is 50.51%–85.24%. The macrolithotype of coal rocks is mainly semi-dull type and semi-bright type. The vitrinite content is between 18.58%–87.75%, the inertinite content is 11.15%–79.78%, and the liptinite content ranges 0–4.27%.

2.2 Experimental testing

Triaxial mechanical compression experiments were conducted on the MTS815.02 Electro-hydraulic Servo-controlled Rock Mechanics Test system of State Key Laboratory for Geomechanics and Deep Underground Engineering of China University of Mining and Technology. The experimental confining pressure is set at 4–45 MPa. The processed standard samples of Φ 50 mm × 100 mm size (drilled parallel to the seam bedding direction) were dried for 24 h at a constant temperature of 65°C in a drying oven. Subsequently, the coal samples were wrapped in a hot melt adhesive membrane to prevent hydraulic oil penetration into the samples during the triaxial compression process, which helped to determine the mechanical properties of the coal accurately. The wrapped coal samples were placed in the triaxial chamber, followed by the installation of stress sensor and oil injection, then the confining pressure ($\sigma_2 = \sigma_3$) and axial pressure were applied at 25°C. The loading rate of confining pressure was 0.1 MPa/s when the confining pressure is less than 15 MPa, while 0.2 MPa/s when the confining pressure was greater than 15 MPa. The axial strain was the control variable of the triaxial experiment until sample failure occurred at the axial strain rate of 2 × 10^{-5}/s, to obtain the complete stress-strain curve of the coal samples.

3 Results

3.1 Stress-strain curves

The stress-strain curve of each coal sample is obtained through real-time monitoring of the triaxial compression process (Fig. 2). The deformation and compression behaviors are similar for coal samples of different ranks. The axial stress and maximum axial strain of coal samples of different ranks show an increasing trend with the confining pressure, divided into five stages: compaction phase, elastic deformation, inelastic deformation, fracture and fracture development, and residual (You, 2003). In the elastic deformation stage, the slope of the curve of low-rank coal samples (TT, SP) with $R_{o,max}$ < 0.65% shows little change, whereas medium-rank coal samples (0.65% < $R_{o,max}$ < 2.5%), and high-rank coal samples ($R_{o,max}$ > 2.5%) show significant change.

3.2 Elastic modulus

The average modulus recommended by the International Society for Rock Mechanics (ISRM) is used to calculate the elastic modulus of the coal sample. The average modulus reflects the slope of the stress-strain curve of the coal sample in the elastic deformation stage. The average modulus of the coal sample has more mechanical significance than the tangent modulus and secant modulus because it excludes the effects of the compaction phase and the inelastic deformation stage (Małkowski and Ostrowski, 2017).

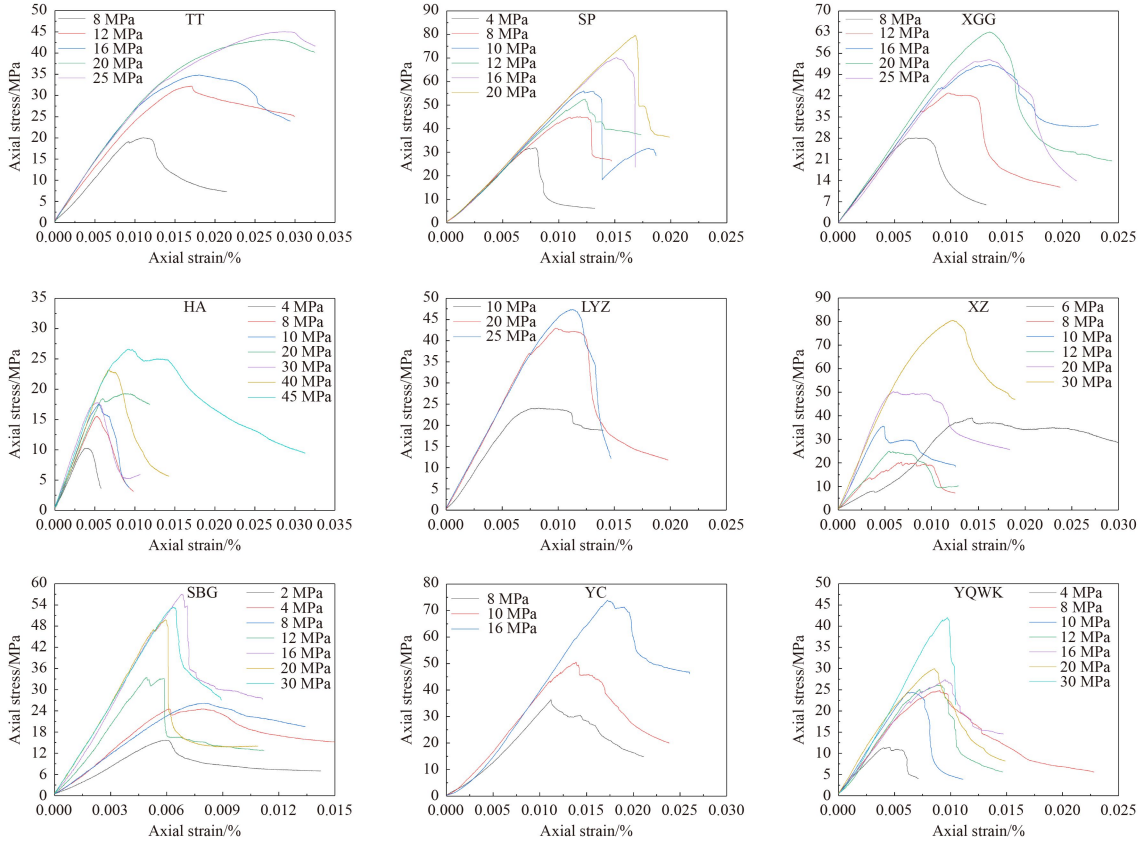

Fig. 2 Stress-strain curves of coal samples under different confining pressure conditions.

Under the same experimental conditions, the elastic modulus of the coal samples have a trend of rapid increase at first, then increase slowly with the confining pressure, thus showing a nonlinear relationship with the confining pressure (Fig. 3(a)). The elastic modulus of coal samples of different ranks varies significantly between 2.25–10.20 GPa (Table 2), with higher elastic modulus for the medium-ranked coal samples and lower elastic modulus for the low-ranked and high-ranked coal samples.

3.3 Compressive strength

The compressive strength of the coal sample is calculated according to the national standard GB/T 23561.9-2009. It is the ratio of the maximum breaking load of the coal sample to the compressed area of the coal sample. Under the same experimental environment, the compressive strengths of different coal ranks vary greatly, ranging from 10.2 to 80.5 MPa (Table 2). The compressive strength of the coal tends to increase with the confining pressure showing a linear relationship (Fig. 3(b)).

3.4 Poisson ratio

The International Society for Rock Mechanics (ISRM) average method is used to calculate the Poisson's ratio of the coal sample. It is the slope of the straight-line portion of the transverse axial strains in the elastic deformation stage, which excludes the influence of the compaction phase on the calculation of Poisson's ratio of coal samples under the effect of confining pressure (Medhurst

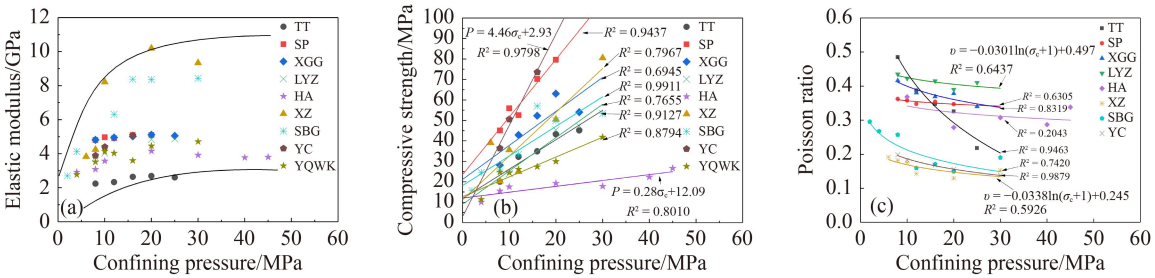

Fig. 3 Relationship between coal mechanical parameters and confining pressure of different coal ranks. (a) Elastic modulus. (b) Compressive strength. (c) Poisson ratio.

and Brown, 1998).

Under the same experimental conditions, the Poisson's ratio of coal tends to decrease with the confining pressure showing a negative logarithmic function (Fig. 3(c)). The Poisson's ratio of coal samples of different ranks varies greatly between 0.130 and 0.485 (Table 2). The coal has a high Poisson ratio and strong lateral deformation ability when $R_{o,max}$ is between 0.34%–1.54% (Tschoegl et al., 2002); however, the Poisson ratio of coal is relatively low and shows weak lateral deformation ability at $R_{o,max} > 1.54\%$.

4 Discussion

4.1 Relationship between the coal mechanical properties and coal rank

The relationships of moisture content, porosity and fracture density with coal ranks are studied to explain the coalification process (Fig. 4).

Table 2 The test results of triaxial mechanics

Samples	σ_c/MPa	P/MPa	E/GPa	υ	Samples	σ_c/MPa	P/MPa	E/GPa	υ
TT	8	20.0	2.25	0.485	SP	8	45.1	4.87	0.362
	12	32.2	2.50	0.387		10	55.9	4.95	0.358
	16	34.9	2.73	0.347		12	52.6	5.00	0.348
	20	43.2	2.69	0.326		16	70.2	5.14	0.354
	25	45.0	2.78	0.218		20	79.6	5.05	0.347
XGG	8	28.1	4.77	0.416	SYFD	10	22.1	4.73	0.214
	12	42.9	4.88	0.380		20	23.6	5.60	0.479
	16	52.3	5.07	0.369		30	48.1	6.14	0.288
	20	63.0	5.13	0.378		40	30.8	5.84	0.267
	25	54.0	5.05	0.340		45	43.6	6.31	0.247
LYZ	10	24.02	3.88	0.454	YC	8	36.4	3.89	0.199
	20	45.35	4.83	0.389		10	50.5	4.40	0.183
	25	47.2	4.87	0.410		16	73.6	5.07	0.168
HA	4	10.2	2.85	0.364	YQWK	4	11.4	2.78	—
	8	15.5	3.10	0.147		8	24.8	3.52	—
	10	17.6	3.50	0.375		10	24.4	4.14	—
	20	19.3	4.14	0.279		12	26.1	4.03	—
	30	17.8	3.91	0.307		16	27.4	3.60	—
	40	22.3	3.75	0.287		20	29.9	4.46	—
	45	26.6	3.73	0.338		30	38.3	4.71	0.411
DZ	10	39.0	8.51	0.325	WZ	10	15.4	3.30	0.437
	20	41.3	9.36	0.357		20	28.5	4.19	0.376
	30	56.9	9.28	0.414		30	14.7	3.36	0.474
	40	57.3	9.66	0.299		40	60.1	4.98	0.365
	45	50.6	7.00	0.466		45	41.8	4.83	0.363
SBG	2	15.7	2.94	0.295	XZ	6	39.1	3.83	0.191
	4	24.5	4.48	0.268		8	20.3	4.25	0.182
	8	26.2	3.97	0.257		10	35.6	8.22	0.175
	12	33.4	7.32	0.159		12	25.0	4.37	0.143
	16	57.0	8.80	0.171		20	50.5	10.20	0.130
	20	49.9	8.83	0.150		30	80.5	9.34	0.153
	30	53.3	8.79	0.190		—	—	—	—

Notes: σ_c, confining pressure, MPa; P, compressive strength, MPa; E, Elastic Modulus, GPa; υ, Poisson Ratio, %. The data of samples SYFD, DZ, and WZ is cited from Zhang et al. (2020c).

4.1.1 Relationship between coal moisture content and coal rank

The oxygen-containing functional groups of the organic matter in the coal decreases gradually before the first coalification jump, therefore during compaction in the coalification process, the moisture content of coal decreases rapidly with the increase in coal rank (Fig. 4(a)) (Xin et al., 2019; Yan et al., 2021). The change in moisture content between the first and third coalification jump is non-significant. However, the moisture content increases rapidly after the third coalification jump due to the thermal cracking of methyl and hydroxyl groups on the coal chemical framework (Bustin and Guo, 1999; Guo and Guo, 2018; Zhang et al., 2019b; Yan et al., 2021).

4.1.2 Relationship between coal porosity and coal rank

The porosity percent of coal samples (Fig. 4(b)) is derived from the helium porosity measurement and in corroboration with the experimental results of Rodrigues (Rodrigues and Lemos de Sousa , 2002). The results show that the porosity of coal decreases rapidly with increasing degree of coalification and compaction of the overlying strata before the first coalification jump (Xin et al., 2019; Lin et al., 2022). Between the first and second transition points, the coal porosity reaches to minimum due to aromatization and bituminization of the coal (Zhou et al., 2017; Zhou et al., 2018). After the third coalification jump, the coal has a high degree of evolution, and the porosity of coal tends to increase due to thermal cracking and debituminization (Rodrigues and Lemos de Sousa, 2002; Zhang et al., 2018; Zhou et al., 2018).

4.1.3 Relationship between coal fracture density and coal rank

Figure 4(c) shows that the fracture density of different coal ranks is distributed in normalized manner and reaches the maximum at the vitrinite reflectance of 1.3% (Bi et al., 2001). Before the first transition point, the coal seam fractures were not developed due to the compaction of the overlying strata (Zhou et al., 2017). Between the first and second transition points, the coal matrix shrinks due to coalification, and the internal stress increases, resulting in an increase in the density of coal fissures. At the same time, the fluid generated in the process of coalification cannot be discharged from the coal seam in time, resulting in fluid pressure and superimposed on internal stress and generates a large number of fractures (Wang et al., 2019; Bi et al., 2001). After the second transition point, the fracture density gradually decreases under the action of the overlying rock pressure due to the decrease in internal stress and hydrocarbon production, which leads to the re-aggregation of the macromolecular functional groups in the coal (Laubach et al., 1998; Dawson and Esterle, 2010).

4.2 Relationship between coal elastic modulus and confining pressure

Different function models (power function; arctangent function; exponential function) describe the nonlinear relationship of the coal elastic modulus with increasing confining pressure (Hobbs et al., 1960; Małkowski and Ostrowski, 2017; Zhang et al., 2020b). In this study, the overall fit of the power function model is not high. The correlation coefficient (R^2) is between 0.5294 and 0.9735, with an average of 0.7623. In the power function model, the fitting degree of the elastic modulus with the confining pressure is low for HA coal ($R_{o,max}$ = 1.54%) and XZ coal ($R_{o,max}$ = 1.88%) shown in Fig. 5(a). The arctangent function model does not fit the elastic modulus of low-rank coals. In the arctangent model, when $R_{o,max}$ = 0.97% and 1.88%, the elastic modulus fit is poor with the confining pressure for LYZ coal ($R_{o,max}$ = 0.97%) and XZ coal ($R_{o,max}$ = 1.88%) illustrated in Fig. 5(b). Whereas the relationship between elastic modulus and confining pressure of coal samples of different ranks is better explained by exponential function model (Table 3, Fig. 5(c)) with the following equation:

$$E = -Ae^{\beta\sigma_c} + E_{max}, \quad (1)$$

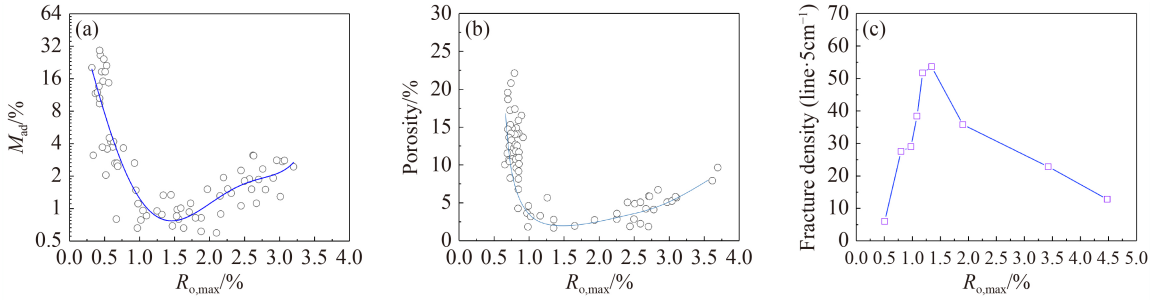

Fig. 4 Relationship between coal mechanical properties and coal rank. (a) Moisture content (Bustin and Guo, 1999; Guo and Guo, 2018; Zhang et al., 2019b; Yan et al., 2021). (b) Porosity (Rodrigies and Lemos de Sousa, 2002). (c) Fracture density (Bi et al., 2001).

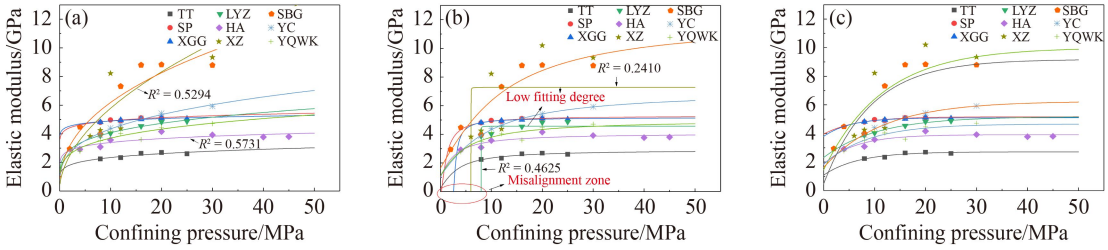

Fig. 5 Relationship between coal elastic modulus and confining pressure in different function models. (a) Power function; (b) Arctangent function; (c) Exponential function.

where E is the elastic modulus under a certain confining pressure, GPa. A and β are the elastic modulus fitting coefficients. A is related to the properties of coal and expressed in GPa. β reflects the sensitivity of the coal elastic modulus to the confining pressure and is expressed as MPa^{-1}. The larger the β, the stronger is the coal sample sensitivity to the confining pressure. σ_c is the confining pressure, MPa. E_{max} is the elastic modulus of coal when the confining pressure approaches infinity, GPa.

The elastic modulus fitting coefficient A of various coal ranks is between 1.46–8.72 GPa, and the fitting coefficient β is between −0.076– −0.227 MPa^{-1}. The maximum elastic modulus E_{max} of different coal ranks is more discrete, ranging from 2.79 to 9.83 GPa. The correlation coefficient R^2 is between 0.6155 and 0.9981, mostly are higher than 0.83 show a high correlation (Table 3).

Figure 6 shows the relationship of coal elastic modulus to the $R_{o,max}$ within the range of coal ranks studied. The trend line in Fig. 6 shows two maximum values, one is at $R_{o,max}$ = 0.70%, and the other is at $R_{o,max}$ = 2.30%, and a minimum point at $R_{o,max}$ = 1.40%, which are almost consistent with the positions of the first, second, and third coalification jumps mentioned by Niu et al. (2019).

Before the first coalification jump, the oxygen-containing functional groups of the organic matter in the coal decreased gradually. During compaction in the coalification process, the water content drops sharply, and the coal porosity gradually decreases (Bustin and Guo, 1999; Tao et al., 2018). A decrease in water content leads to an increase in the frictional resistance of the coal slip surface (Tao et al., 2018; Liu et al., 2021). While, the decrease in porosity further increases the coal's ability to resist deformation, resulting in an increasing trend of in the coal elastic modulus (Zhou et al., 2016; Yao et al., 2020; Liu et al., 2021) (Figs. 4(a) and 4(b)). Between the first and second transition points, the water content of coal no longer changes significantly (Zhang et al., 2019a; Yan et al., 2021). However due to the influence of overburden pressure during asphaltization, aromatization, and coalification, the density of internal coal fractures gradually increases to about $R_{o,max}$ = 1.3%, when the density of endogenous fissures reach the maximum, the porosity of coal decreases to the minimum (Fig. 4(c)); as a result, the endogenous fissures of coal are well developed (Bi et al., 2001; Niu et al., 2019). The plasticity of coal increases, the resistance to deformation decreases, and the elastic modulus shows a decreasing trend. Between the second and third coalification jump, the density of endogenous fractures of coal continues to decrease (Bi et al., 2001), the rigidity of coal increases along with the increase in the elastic modulus of coal. After the third transition point, due to thermal cracking, the methyl and

Table 3 Fitting relationships of elastic modulus and confining pressure for various coal ranks

Samples	$R_{o,max}$/%	Fitting equation	/GPa	β/MPa^{-1}	E_{max}/GPa	R^2
TT	0.34	$E = -1.63e^{-(\sigma_c/6.73)} + 2.71$	1.63	−0.149	2.71	0.8352
SP	0.59	$E = -1.21e^{-(\sigma_c/6.43)} + 5.20$	1.21	−0.156	5.16	0.8579
XGG	0.67	$E = -1.31e^{-(\sigma_c/5.23)} + 5.10$	1.31	−0.191	5.10	0.9211
LYZ	0.97	$E = -2.86e^{-(\sigma_c/10.37)} + 5.17$	2.86	−0.096	5.17	0.9862
HA	1.54	$E = -2.07e^{-(\sigma_c/6.14)} + 3.91$	2.07	−0.163	3.88	0.8174
SYFD	1.59	$E = -4.08e^{-(\sigma_c/9.70)} + 6.15$	4.08	−0.103	6.15	0.9119
DZ	1.63	$E = -4.09e^{-(\sigma_c/6.14)} + 9.54$	4.09	−0.163	9.54	0.9129
WZ	1.73	$E = -3.48e^{-(\sigma_c/14.69)} + 5.07$	3.48	−0.068	5.07	0.9981
XZ	1.88	$E = -8.72e^{(\sigma_c/9.27)} + 9.18$	8.72	−0.108	9.18	0.6155
SBG	1.97	$E = -8.56e^{-(\sigma_c/13.20)} + 10.01$	8.56	−0.086	10.01	0.8793
YC	2.80	$E = -4.52e^{-(\sigma_c/12.28)} + 6.32$	4.52	−0.081	6.32	0.9980
YQWK	3.04	$E = -2.83e^{-(\sigma_c/8.74)} + 4.66$	2.61	−0.114	4.34	0.7818

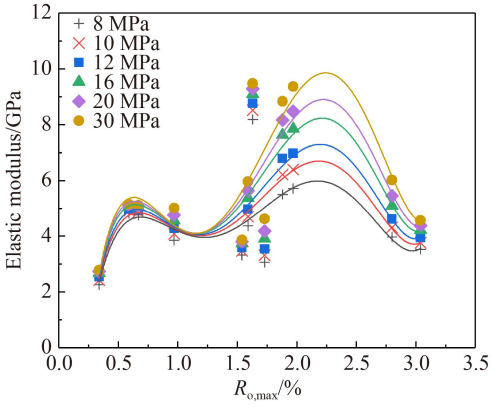

Fig. 6 Relationship between coal elastic modulus of different confining pressures and $R_{o,max}$.

hydroxyl groups on the coal chemical framework fall off on a large scale, and the water content of the coal seam further increases (Bustin and Guo, 1999; Guo and Guo, 2018; Zhang et al., 2019a; Yan et al., 2021), which enhances the plasticity of coal, reduces the coal particles adhesion ability, and decreases the rigidity of coal and rock. At the same time, the molecular structure of coal changes is affected by coalification and tectonics, and the porosity gradually increases (Rodrigues and Lemos de Sousa 2002; Zhou et al., 2018). When the coal is under overburden pressure, it is more prone to deformation, and the elastic modulus of coal decreases (Figs. 4(a) and 4(b)).

The maximum elastic moduli of different coal ranks vary significantly (Table 3). The influence of confining pressure on the elastic modulus of different coal ranks is compared using the following equation:

$$E_w = \frac{E_i}{E_{\max}}, \tag{2}$$

where E_w is the dimensionless elastic modulus of coal samples. E_i is the elastic modulus of each confining pressure point, GPa.

The sensitivity of the elastic modulus of different coal ranks to the confining pressure and the overlying rock pressure is studied using the following equation:

$$\beta_k = \frac{\partial E_w}{\partial \sigma_c} = \frac{1}{E_{\max}} \frac{\partial E_i}{\partial \sigma_c}, \tag{3}$$

where β_k elastic modulus stress sensitivity coefficient, MPa^{-1}, a coefficient represents the change of the elastic modulus of the coal sample under the condition of unit confining pressure. The high value of β_k represents that the elastic modulus is easily affected by the confining pressure and shows greater sensitivity of the coal elastic modulus.

The sensitivity coefficients of elastic modulus of different coal ranks decrease with increased confining pressure (Fig. 7). Under the condition of low confining pressure (< 20 MPa), the pores and fractures of the coal sample are quickly compressed and closed, the elastic modulus increases sharply, and the sensitivity to the confining pressure is the greatest. Under the condition of high confining pressure (> 20 MPa), the pores and fractures in the coal have been compressed and closed, and the elastic modulus of the coal sample is gradually approaching the maximum value, the confining pressure has little effect on the elastic modulus of the coal sample, and the sensitivity coefficient of the elastic modulus tends to be zero.

The relationship between the sensitivity coefficient β_k of the elastic modulus at 8–30 MPa of confining pressure and the coal ranks is analyzed. The results show a maximum point and a minimum point for β_k with the increase in coal rank (Fig. 8). The minimum point of β_k is at $R_{o,max}$ = 0.70% and the maximum point is at $R_{o,max}$ = 2.40%, which are nearly consistent with the position of the first and third transition points of coal (Tschoegl et al., 2002).

The coal structure is elastic and has weak planes (Wang et al., 2017). Before the first coalification jump, porosity

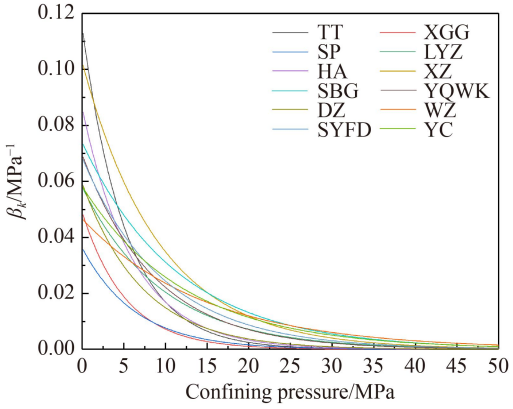

Fig. 7 Relationship between elastic modulus sensitivity coefficient of different coal ranks and the confining pressure.

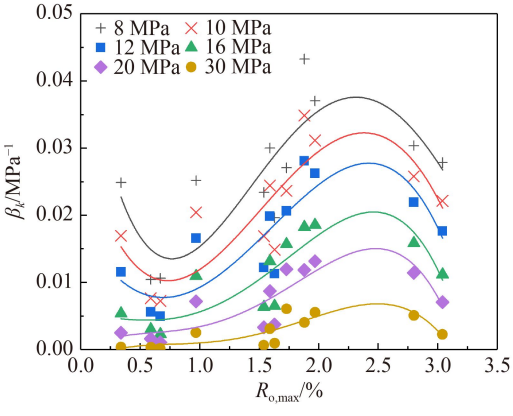

Fig. 8 Relationship between elastic modulus sensitivity coefficients and coal ranks ($R_{o,max}$, %) at different confining pressures.

in the coal decreases sharply along with the decrease in the proportion of macropores. At the same time, the fractures are extremely undeveloped (Bi et al., 2001; Rodrigues and Lemos de Sousa, 2002; Xin et al., 2019) (Figs. 4(a) and 4(c)), and the number of weak planes in the internal defect structure of the coal is small, and the coal body tends to be completely elastic (Xin et al., 2019; Zhang et al., 2020a), and the confining pressure has little effect on the deformation of the elastic body. Therefore, the coal elastic modulus is not sensitive to the confining pressure, and the sensitivity coefficient of the coal elastic modulus tends to decrease. Fractures develop in the coal with the coalification transition between the first and third transition points. However, the porosity increases near the third transition point to increase the coal compressibility, consistent with the compression coefficient curve of coal pores and fractures in the overburden coal porosity experiment (Rodrigues and Lemos de Sousa, 2002; Ma et al., 2020) (Fig. 9), therefore the sensitivity coefficient of coal elastic modulus increases. After the third transition point, the coal porosity increases, but the proportion of micropores increases and the proportion of macropore decreases (Wang et al., 2014); therefore, the compressibility of coal decreases along with the decrease in the sensitivity of coal elastic modulus.

4.3 Strength characteristics analysis and strength criteria

The compressive strength of the coal sample has a linear relationship with the confining pressure (Fig. 3(b)). The pores and fissures of the coal are compressed and closed under the action of the confining pressure; therefore, the coal resistance to deformation and the compressive strength of coal samples are increased. The vertical normal stress component of the coal fracture surface increases with the confining pressure, and the friction resistance also increases, which inhibits the relative sliding between the fracture surfaces and improves the triaxial compressive strength of the coal sample (Kong and Wang, 2014).

The compressive strength of coal has two maximum points at $R_{o,max}$ = 0.70% and 2.70%, and one minimum point at $R_{o,max}$ = 1.30%, respectively, with the increase in coal rank (Fig. 10), Nearly consistent with the first, second, and third transition points of coal (Niu et al., 2019). Before the first coalification jump, the water content and porosity of the coal show a downward trend with the increase in coal rank, which enhances the frictional resistance of the weak plane in the coal and the ability of the coal to resist deformation (Rodrigues and Lemos de Sousa, 2002; Palchik and Hatzor, 2004; Xin et al., 2019; Zhang and Nie, 2020), and increase the compressive strength of coal. Between the first and the second coalification jump, the fracture density of coal increases with the increase in coal rank, which increases the weak plane in the coal and decreases the compressive strength of the coal and its deformation resistance ability (Bi et al., 2001; Li et al., 2020). Between the second and the third coalification jump, the fracture density of the coal gradually decreases to increase the deformation resistance and the compressive strength of coal. After the third transition point, the water content and porosity of coal increases with the coal rank. Moisture reduces the cohesive ability between coal particles, softens the clay and other minerals in the coal, thus weakening the compressive capacity of the coal and reducing the frictional resistance of the weak plane of the coal to decrease its deformation resistance ability. On the other hand, the increase in porosity also dramatically decreases the deformation resistance ability of the coal and its compressive strength (Bi et al., 2001; Braga et al., 2019; Zhang et al., 2019b; Yan et al., 2021).

In the triaxial experiment, when $\sigma_2 = \sigma_3 = \sigma_c$, the coal strength criterion satisfies the given equation (Liu et al., 2017):

$$\sigma_1 = f(\sigma_c), \tag{4}$$

where σ_1 represents the maximum axial stress, and σ_c is the confining pressure applied on the coal sample. The

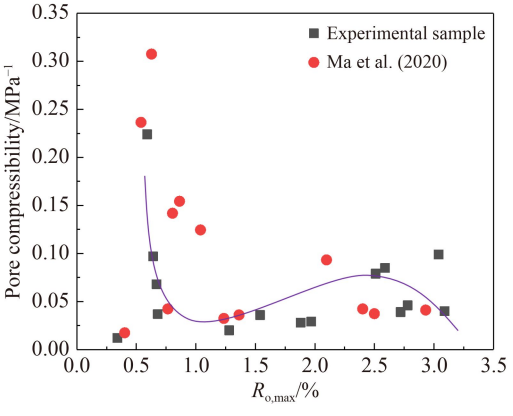

Fig. 9 Correlation of pore compressibility with different coal ranks ($R_{o,max}$, %).

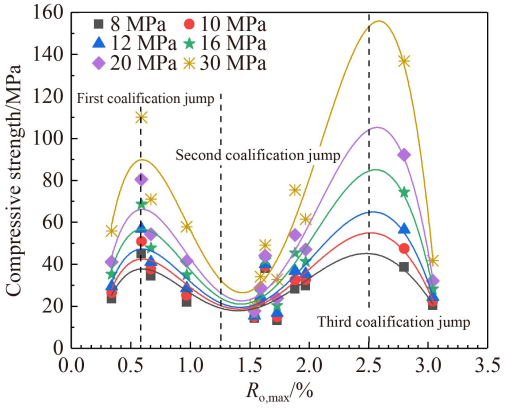

Fig. 10 Relationship between coal ranks ($R_{o,max}$, %) and coal compressive strength at different confining pressures.

compressive strength of coal has a strong linear relationship with the confining pressure, which can be expressed as (Zhang et al., 2020a)

$$\sigma_1 = K\sigma_c + A_0, \tag{5}$$

where A_0 is the compressive strength under no confining pressure fit by the function, MPa. K is the dimensionless compressive strength coefficient. Hence, Eq. (5) is transformed to determine the strength criterion of the principal stress form of coal as follows:

$$\frac{\sigma_1}{A_0} = \frac{K}{A_0}\sigma_c + 1 = K_1\sigma_c + 1, \tag{6}$$

where K_1 is the fitting strength coefficient, which characterizes the increase in compressive strength as the confining pressure increases. The strength criteria of different coal ranks can be obtained by substituting the compressive strength and confining pressure data of different coal samples into Eq. (6) given in Table 4. The maximum shear stress of coal and rock is determined from the bonding force and the angle of internal friction using Mohr-Coulomb strength theory as follows:

$$\tau = C + \sigma\tan\varphi, \tag{7}$$

where τ represents the shear strength of coal, MPa. φ represents the internal friction angle of coal. σ represents the normal stress perpendicular to the shear plane, MPa. C represents the bonding force, MPa. The parameters K and A_0 in Eq. (5) and the parameters C and φ in Eq. (7) satisfy the following equation (Zhang et al., 2019a; Yan et al., 2021):

$$K = \frac{1+\sin\varphi}{1-\sin\varphi},\ A_0 = \frac{2C\cos\varphi}{1-\sin\varphi}. \tag{8}$$

According to Eq. (8), the internal friction angle and cohesive force of coal can be calculated as follows:

$$\varphi = \sin^{-1}\frac{K-1}{K+1},\ C = \frac{A_0}{2\sqrt{K}}. \tag{9}$$

According to the fitting relationship between the compressive strength of coal and the confining pressure, the parameters and strength criteria of different coal ranks are calculated using Eqs. (4) to (9) (Table 4). The strength characteristics of the experimental coal samples have a linear relationship with the confining pressure. Therefore, the failure characteristics of coal samples of different ranks conform to the Coulomb failure criterion. The internal friction angle φ of the experimental coal sample is between 0.91° and 39.33°, which increases with the compressive strength coefficient K. The cohesive force C is from 0.69 to 28.04 MPa. The internal friction angle and cohesive force are related to the fitted compressive strength A_0 and the compressive strength coefficient K under the condition of no confining pressure, but not highly correlated with $R_{o,max}$.

4.4 Influence of coalification jump on fracturing effect

The molecular structure and the physical properties of the coal reservoir changed during coalification, subsequently altering the mechanical properties of various coal ranks. The mechanical properties of coal reservoirs are critical in the hydraulic fracturing of coal. The fracture initiation pressure and fracture propagation pattern required for hydraulic fracturing are affected by the elastic modulus and compressive strength of the coal seam (Kang et al., 2010; Fan et al., 2019). The shape and size of fractures depend upon the elastic modulus of the coal during hydraulic fracturing (Kang et al., 2010; Weng et al., 2011; Yang et al., 2012). When the elastic modulus of the coal is higher, narrower and shorter fractures tend to be formed (Li et al., 2014; Liu et al., 2022), whereas the lower the elastic modulus of the coal, the shorter and

Table 4 Criteria and parameters of coal stress intensity of different coal ranks

Samples	φ/(°)	C/MPa	K_1	K	A_0/MPa	Shear stress failure criterion	Principal stress failure criterion
TT	10.33	4.92	0.1219	1.4370	11.79	$\tau = 4.92 + 0.1823\sigma$	$\sigma_1/A_0 = 0.1219\sigma_3 + 1$
SP	28.42	6.99	0.1200	2.8168	23.48	$\tau = 6.99 + 0.5412\sigma$	$\sigma_1/A_0 = 0.1382\sigma_3 + 1$
XGG	14.40	8.20	0.0786	1.6623	21.14	$\tau = 8.20 + 0.2568\sigma$	$\sigma_1/A_0 = 0.0786\sigma_3 + 1$
LYZ	13.85	3.52	0.1813	1.6293	8.99	$\tau = 3.52 + 0.2466\sigma$	$\sigma_1/A_0 = 0.1813\sigma_3 + 1$
HA	33.74	6.60	0.0235	0.2843	12.09	$\tau = 6.60 + 0.6679\sigma$	$\sigma_1/A_0 = 0.0235\sigma_3 + 1$
SYFD	17.91	15.32	0.0290	0.5297	18.27	$\tau = 15.32 + 0.3232\sigma$	$\sigma_1/A_0 = 0.0129\sigma_3 + 1$
DZ	19.26	28.04	0.0148	0.5039	33.98	$\tau = 28.04 + 0.3494\sigma$	$\sigma_1/A_0 = 0.0148\sigma_3 + 1$
WZ	3.30	5.89	0.1469	0.8911	6.07	$\tau = 5.89 + 0.0577\sigma$	$\sigma_1/A_0 = 0.0147\sigma_3 + 1$
XZ	21.29	3.81	0.1920	2.1404	11.15	$\tau = 3.81 + 0.3897\sigma$	$\sigma_1/A_0 = 0.1920\sigma_3 + 1$
SBG	10.51	7.54	0.0797	1.4464	18.14	$\tau = 7.54 + 0.1855\sigma$	$\sigma_1/A_0 = 0.0797\sigma_3 + 1$
YC	39.33	0.69	1.5236	4.4614	2.92	$\tau = 0.69 + 0.8194\sigma$	$\sigma_1/A_0 = 1.5236\sigma_3 + 1$
YQWK	0.91	7.14	0.0762	0.9689	12.71	$\tau = 7.14 + 0.0159\sigma$	$\sigma_1/A_0 = 0.0762\sigma_3 + 1$

wider fractures will be developed (Li and Li, 2021).

Before the first coalification transition; the elastic modulus and compressive strength of coal showed an upward trend, the fracture initiation pressure of the coal seam increased with the increase of coal rank, and the fractures transitioned from wide to narrow in size. Between the first and second transition points; the elastic modulus and compressive strength of the coal showed a downward trend, the fractures in the coal were highly developed, a minor fracture initiation pressure can form a favorable fracture network for drainage, fractures transitioned from narrow to wide in size, and an appropriate proppant was selected to prevent the fractures from opening and closing (Ahamed et al., 2021; Zhang et al., 2021). Between the second and third transition points; the elastic modulus and compressive strength of the coal showed an upward trend, the fracture density in the coal gradually decreased, the fracture initiation pressure required for fracturing the coal seam increased, and the fracture shape transitioned to the narrow type. After the third transition point; the elastic modulus and compressive strength of coal decreased rapidly, the fracturing pressure required for fracturing the coal seam decreased, and the fracture shape tended to be short and wide (Figs. 6 and 10).

5 Conclusions

1) The slope of the stress-strain curve of low-rank coal changes non-significantly than high-rank coal at the elastic deformation stage. The compressive strength of different coal ranks is linearly related to the confining pressure; the elastic modulus and the confining pressure have a positive exponential function, whereas the Poisson's ratio has a negative logarithmic relationship with the confining pressure.

2) The elastic modulus and compressive strength of coal are "M" shape with the increase in coal rank, and the transition points are located at $R_{o,max}$ = 0.70%, 1.30%, and 2.40%, which are consistent with the first, second and the third coalification jump point positions, respectively. The elastic modulus and compressive strength increased before the first coalification jump, and these tend to decrease and then increase between the first and third transition points, whereas after the third transition point, the elastic modulus and compressive strength decreased.

3) The sensitivity coefficient of elastic modulus showed an inverted "S" shape with the increasing coal rank, and the transition points are located at $R_{o,max}$ = 0.70% and 2.40%. It is almost consistent with the first and third coalification jump point positions, respectively. Coal porosity decreases before the first transition point, whereas the elastic modulus is less sensitive to the confining pressure. Coal sensitivity increases between the first and third transition points, whereas it decreases after the third transition point.

4) The strength characteristics of coal samples of different ranks have a linear relationship with the confining pressure. The internal friction angle is between 0.91° and 39.33°, and the cohesion is between 0.69 and 28.04 MPa. The Coulomb strength criterion can characterize the destruction of coals of different ranks.

Acknowledgments This study was supported by the National Natural Science Foundation of China (Grant Nos. 42072191 and 42072190) and Hebei Natural Science Foundation Project (No. E2020209074) and Shanxi Province Science and Technology Plan unveiling and bidding project (No. 20201101003) and Prospective Basic Technology Key Project of CNPC during the "Fourteenth Five-Year Plan" (No. 2021DJ2302). At the same time, we would like to sincerely appreciate the editors and anonymous reviewers for their valuable comments.

References

Ahamed M, Perera M, Elsworth D, Ranjith P, Matthai S, Dongyin L (2021). Effective application of proppants during the hydraulic fracturing of coal seam gas reservoirs: implications from laboratory testings of propped and unpropped coal fractures. Fuel, 304: 121394

Bi J, Su X, Han D, Chen J (2001). The relation between cleat frequency and coal rank. J China Coal Soc, 26(4): 346–349 (in Chinese)

Braga E, Silva G, Amaral R, Carias M, Assis P, Lemos L (2019). Influence of moisture and particle size on coal blend bulk density. REM Int Eng J, 72(2): 237–242

Bustin R, Guo Y (1999). Abrupt changes (jumps) in reflectance values and chemical compositions of artificial charcoals and inertinite in coals. Int J Coal Geol, 38(3–4): 237–260

Dawson G, Esterle J (2010). Controls on coal cleat spacing. Int J Coal Geol, 82(3–4): 213–218

Fan C, Li S, Luo M, Yang Z, Lan T (2019). Numerical simulation of hydraulic fracturing in coal seam for enhancing underground gas drainage. Energy Explor Exploit, 37(1): 166–193

Gentzis T, Deisman N, Chalaturnyk R J (2007). Geomechanical properties and permeability of coals from the Foothills and Mountain regions of western Canada. Int J Coal Geol, 69(3): 153–164

Hobbs D (1960). The strength and stress-strain characteristics of oakdale coal under triaxial compression. Geol Mag, 97(5): 422–435

Hou H, Shao L, Tang Y, Zhao S, Yuan Y, Li Y, Mu G, Zhou Y, Liang G, Zhang J (2020). Quantitative characterization of low-rank coal reservoirs in the southern Junggar Basin, NW China: implications for pore structure evolution around the first coalification jump. Mar Pet Geol, 113: 104165

Jiang T, Zhang J, Wu H (2016). Experimental and numerical study on hydraulic fracture propagation in coalbed methane reservoir. J Nat Gas Sci Eng, 35(9): 455–467

Kong H, Wang L (2014). Influence on coal rock strength and deformation of confining pressure. Electron J Geotech Eng, 19: 3575–3585

Li D, Zhang S, Zhang S (2014). Experimental and numerical simulation study on fracturing through interlayer to coal seam. J Nat Gas Sci Eng, 21: 386–396

Li H, Liang W, Wang J, Cao W, Wu P, Ma K, Wei J, Li J (2021). Research on main controlling factors and its influencing laws on hydraulic fracture network in the fractured soft and low-permeability coal. J Nat Gas Sci Eng, 95(11): 104147

Li J, Li B (2021). Modeling of anisotropic coal permeability under the effects of matrix-fracture interaction. J Nat Gas Sci Eng, 93: 104022

Li S, Ni G, Wang H, Xun M, Xu Y (2020). Effects of acid solution of different components on the pore structure and mechanical properties of coal. Adv Powder Technol, 31(4): 1736–1747

Lin Y, Qin Y, Qiao J, Li G, Zhang H (2022). Effect of coalification and maceration on pore differential development characteristics of high-volatile bituminous coal. Fuel, 318: 123634

Liu J, Yao Y, Liu D, Xu L, Elsworth D, Huang S, Luo W (2018). Experimental simulation of the hydraulic fracture propagation in an anthracite coal reservoir in the southern Qinshui Basin, China. J Petrol Sci Eng, 168(9): 400–408

Liu N, Li C, Feng R, Xia X, Gao X (2021). Experimental study of the influence of moisture content on the mechanical properties and energy storage characteristics of coal. Geofluids, 2021: 6838092

Liu Q, Cheng Y, Jin K, Tu Q, Zhao W, Zhang R (2017). Effect of confining pressure unloading on strength reduction of soft coal in borehole stability analysis. Environ Earth Sci, 76(4): 173

Liu Y, Tang D, Xu H, Zhao T, Hou W (2022). Effect of interlayer mechanical properties on initiation and propagation of hydraulic fracturing in laminated coal reservoirs. J Petrol Sci Eng, 208: 109381

Ma R, Wang M, Bake A, Jia T, Zhu J (2020). Experimental study of overburden pore porosity and permeability of low-rank coal reservoirs in southeastern Junggar. J China Univ Min Technol, 49(06): 1182–1192

Małkowski P, Ostrowski Ł (2017). The methodology for the Young modulus derivation for rocks and its value. Procedia Eng, 191: 134–141

Masoudian M, Airey D, El-Zein A (2014). Experimental investigations on the effect of CO_2 on mechanics of coal. Int J Coal Geol, 128–129: 12–23

Medhurst T, Brown E (1998). A study of the mechanical behavior of coal for pillar design. Int J Rock Mech Min Sci, 35(8): 1087–1105

Meszaros N, Subedi B, Stamets T, Shifa N (2017). Assessment of surface water contamination from coalbed methane fracturing-derived volatile contaminants in Sullivan County, Indiana, USA. Bull Environ Contam Toxicol, 99(3): 385–390

Niu Q, Pan J, Jin Y, Wang H, Li M, Ji Z, Wang K, Wang Z (2019). Fractal study of adsorption-pores in pulverized coals with various metamorphism degrees using N_2 adsorption, X-ray scattering and image analysis methods. J Petrol Sci Eng, 176(5): 584–593

Palchik V, Hatzor Y H (2004). The influence of porosity on tensile and compressive strength of porous chalks. Rock Mech Rock Eng, 37(4): 331–341

Pan J, Meng Z, Hou Q, Ju Y, Cao Y (2013). Coal strength and Young's modulus related to coal rank, compressional velocity and maceral composition. J Struct Geol, 54(9): 129–135

Peng W, Mao X, Lin J, Du C (2009). Study of the borehole hydraulic fracturing and the principle of gas seepage in the coal seam. In: International Conference on Mining Science & Technology Icmst, 1(1): 1561–1573

Perera S, Ranathunga A, Ranjith P (2016). Effect of coal rank on various fluid saturations creating mechanical property alterations using australian coals. Energies, 9(6): 440

Ranathunga A, Perera M, Ranjith P (2016). Influence of CO_2 adsorption on the strength and elastic modulus of low rank Australian coal under confining pressure. Intern Coal Geol, 167: 148–156

Rodrigues C F, Lemos de Sousa M J (2002). The measurement of coal porosity with different gases. Int J Coal Geol, 48(3–4): 245–251

Su X, Lin X, Song Y, Zhao M (2004). The classification and model of coalbed methane reservoirs. Acta Geol Sin, 78(3): 662–666

Tao S, Chen S, Tang D, Zhao X, Xu H, Li S (2018). Material composition, pore structure and adsorption capacity of low-rank coals around the first coalification jump: a case of eastern Junggar Basin, China. Fuel, 211: 804–815

Tschoegl N, Knauss W, Emri I (2002). Poisson's ratio in linear viscoelasticity – a critical review. Mech Time-Depend Mater, 6(1): 3–51

Wang F, Cheng Y, Lu S, Jin K, Zhao W (2014). Influence of coalification on the pore characteristics of middle–high rank coal. Energy Fuels, 28(9): 5729–5736

Wang K, Du F, Zhang X, Wang L, Xin C (2017). Mechanical properties and permeability evolution in gas-bearing coal–rock combination body under triaxial conditions. Environ Earth Sci, 76(24): 815

Wang Z, Fu X, Pan J, Niu Q, Zhou H, Zhai Y (2019). The fracture anisotropic evolution of different ranking coals in Shanxi Province, China. J Petrol Sci Eng, 182: 106281

Weng X, Kresse O, Cohen C, Wu R, Gu H (2011). Modeling of hydraulic-fracture-network propagation in a naturally fractured formation. SPE Prod Oper, 26(4): 368–380

Xin F, Xu H, Tang D, Yang J, Chen Y, Cao L, Qu H (2019). Pore structure evolution of low-rank coal in China. Int J Coal Geol, 205: 126–139

Xiong X, Cao D, Jiang Y, Bian L, Wang W, Wang L, Liu Q (2014). Application of well temperature logging in coalbed methane well fracture effectiveness evaluation. Appl Mech Mater, 522–524: 1522–1527

Yan J, Meng Z, Li G (2021). Diffusion characteristics of methane in various rank coals and the control mechanism. Fuel, 283: 118959

Yang H, Huo X, Zhang S (2012). Study on difference of outburst elimination effect between sub-layers of soft coal and hard coal under the condition of gas per-drainage. Saf Sci, 50(4): 768–772

Yang Y, Li X, Zhang Y, Mei Y, Ding R (2020). Insights into moisture content in coals of different ranks by low field nuclear resonance. Energy Geosci, 1(3–4): 93–99

Yao Q, Li X, Zhou J, Ju M H, Chong Z H, Zhao B (2015). Experimental study of strength characteristics of coal specimens after water intrusion. Arab J Geosci, 8(9): 6779–6789

Yao Q, Wang W, Zhu L, Xia Z, Tang C, Wang X (2020). Effects of moisture conditions on mechanical properties and AE and IR characteristics in coal–rock combinations. Arab J Geosci, 13(14): 615

You M (2003). Effect of confining pressure on the Young's modulus of rock specimen and the friction in fissures. Rock and Soil Mechanics, 24(S2): 167–170 (in Chinese)

Yu G, Vozoff K, Durney D (1993). The influence of confining pressure and water saturation on dynamic elastic properties of some Permian coals. Geophysics, 58(1): 30–38

Zhang B, Ran X, Wang Y, Zhang F, Liang W, Li Z (2021). Experimental study on mechanical properties of coal rocks in re-fracturing. Alex Eng J, 60(3): 3315–3325

Zhang J, Wei C, Yan G, Lu G (2019b). Structural and fractal characterization of adsorption pores of middle–high rank coal reservoirs in western Yunnan and eastern Guizhou: an experimental study of coals from the Panguan syncline and Laochang anticline. Energy Explor & Exploit, 37(1): 251–272

Zhang L, Li X, Ren T (2020b). A theoretical and experimental study of stress–strain, creep and failure mechanisms of intact coal. Rock Mech Rock Eng, 53(12): 5641–5658

Zhang M, Fu X, Duan C, Li Y (2020c). Influencing factor analysis of the coal matrix compressibility of middle-high rank coals. J Nat Gas Sci Eng, 81: 103462

Zhang M, Fu X, Wang H (2018). Analysis of physical properties and influencing factors of middle-rank coal reservoirs in China. J Nat Gas Sci Eng, 50: 351–363

Zhang M, Nie R (2020). Experimental investigation on the influence of water content on the mechanical properties of coal under conventional triaxial compression. Shock Vib, 2020: 1–11

Zhang P, Meng Z, Zhang K, Jiang S (2020a). Impact of coal ranks and confining pressures on coal strength, permeability, and acoustic emission. Int J Geomech, 20(8): 04020135

Zhang Z, Xie H, Zhang R, Zhang Z, Gao M, Jia Z, Xie J (2019a). Deformation damage and energy evolution characteristics of coal at different depths. Rock Mech Rock Eng, 52(5): 1491–1503

Zhou S, Liu D, Cai Y, Yao Y (2017). Effects of the coalification jump on the petrophysical properties of lignite, subbituminous and high-volatile bituminous coals. Fuel, 199: 219–228

Zhou S, Liu D, Karpyn Z T, Cai Y, Yao Y (2018). Effect of coalification jumps on petrophysical properties of various metamorphic coals from different coalfields in China. J Nat Gas Sci Eng, 60: 63–76

Zhou Y, Li Z, Yang Y, Zhang L, Qi Q, Si L, Li J (2016). Improved porosity and permeability models with coal matrix block deformation effect. Rock Mech Rock Eng, 49(9): 3687–3697